

University of New England

**DUNE: DigitalUNE**

---

Pharmaceutical Sciences Faculty Publications

Pharmaceutical Sciences Faculty Works

---

9-29-2017

## Defining The Epichromatin Epitope

Travis J. Gould

Katalin Tóth

Norbert Mücke

Jörg Langowski

Alexandra S. Hakusui

*See next page for additional authors*

Follow this and additional works at: [https://dune.une.edu/pharmsci\\_facpubs](https://dune.une.edu/pharmsci_facpubs)



Part of the [Pharmacy and Pharmaceutical Sciences Commons](#)

---

---

**Authors**

Travis J. Gould, Katalin Tóth, Norbert Mücke, Jörg Langowski, Alexandra S. Hakusui, Ada L. Olins, and Donald E. Olins

## Defining the epichromatin epitope

Travis J. Gould, Katalin Tóth, Norbert Mücke, Jörg Langowski, Alexandra S. Hokusui, Ada L. Olins & Donald E. Olins

**To cite this article:** Travis J. Gould, Katalin Tóth, Norbert Mücke, Jörg Langowski, Alexandra S. Hokusui, Ada L. Olins & Donald E. Olins (2017) Defining the epichromatin epitope, *Nucleus*, 8:6, 625-640, DOI: 10.1080/19491034.2017.1380141

To link to this article: <https://doi.org/10.1080/19491034.2017.1380141>



© 2017 Taylor & Francis



[View supplementary material](#) 



Accepted author version posted online: 29 Sep 2017.  
Published online: 30 Oct 2017.



Submit your article to this journal 



Article views: 476



[View related articles](#) View Crossmark data 

Citing articles: 4 View citing articles 

ORIGINAL RESEARCH



## Defining the epichromatin epitope

Travis J. Gould<sup>a</sup>, Katalin Tóth<sup>b</sup>, Norbert Mücke<sup>b</sup>, Jörg Langowski <sup>b,†</sup>, Alexandra S. Hakusui<sup>a</sup>, Ada L. Olins<sup>c</sup>, and Donald E. Olins <sup>c</sup>

<sup>a</sup>Department of Physics & Astronomy, Bates College, Lewiston, ME, USA; <sup>b</sup>Division of Biophysics of Macromolecules, German Cancer Research Center (DKFZ), Heidelberg, Germany; <sup>c</sup>Department of Pharmaceutical Sciences, College of Pharmacy, University of New England, Portland, ME, USA

### ABSTRACT

Epichromatin is identified by immunostaining fixed and permeabilized cells with particular bivalent anti-nucleosome antibodies (mAbs PL2-6 and 1H6). During interphase, epichromatin resides adjacent to the inner nuclear membrane; during mitosis, at the outer surface of mitotic chromosomes. By STED (stimulated emission depletion) microscopy, PL2-6 stained interphase epichromatin is ~76 nm thick and quite uniform; mitotic epichromatin is more variable in thickness, exhibiting a “wrinkled” surface with an average thickness of ~78 nm. Co-immunostaining with anti-Ki-67 demonstrates Ki-67 deposition between the PL2-6 “ridges” of mitotic epichromatin. Monovalent papain-derived Fab fragments of PL2-6 yield a strikingly different punctate “chromomeric” immunostaining pattern throughout interphase nuclei and along mitotic chromosome arms. Evidence from electrophoretic mobility shift assay (EMSA) and from analytical ultracentrifugation characterize the Fab/mononucleosome complex, supporting the concept that there are two binding sites per nucleosome. The peptide sequence of the Hv3 region (heavy chain variable region 3) of the PL2-6 antibody binding site strongly resembles other nucleosome acidic patch binding proteins (especially, LANA and CENPC), supporting that the nucleosome acidic patch is included within the epichromatin epitope. It is speculated that the interphase epichromatin epitope is “exposed” with favorable geometric arrangements for binding bivalent PL2-6 at the surface chromatin; whereas, the epitope is “hidden” within internal chromatin. Furthermore, it is suggested that the “exposed” nucleosome surface of mitotic epichromatin may play a role in post-mitotic nuclear envelope reformation.

### ARTICLE HISTORY

Received 6 July 2017  
Revised 9 August 2017  
Accepted 12 September 2017

### KEYWORDS






acidic patch; bivalent antibody; chromomere; confocal; LANA (latency-associated nuclear antigen from Kaposi's Sarcoma Herpesvirus); monovalent fab fragment; nucleosome; STED

## Introduction

The concept of epichromatin (i.e., the surface of chromatin adjacent to the interphase nuclear envelope and on the “outer” surface of mitotic chromosomes) is based upon specific localization in immunostaining experiments.<sup>1,2</sup> Two mouse monoclonal antibodies (PL2-6, obtained from spleen cells of an autoimmune mouse<sup>3</sup>; 1H6, obtained from mice immunized with liposomes containing phosphatidylserine<sup>4</sup>) produce a characteristic and reproducible staining pattern on fixed nuclei and mitotic chromosomes, visualized in a wide range of species spanning from human to plant cells.<sup>1,2</sup>

Ever since the discovery of epichromatin, the questions of what epitope these antibodies are “recognizing” and what might be its structural and functional significance, have been a basis for speculation. At the

onset, given the wide range of species exhibiting the epichromatin epitope, it seemed unlikely that these antibodies are recognizing specific nucleotide sequences. More likely, given the demonstrated strong interactions of PL2-6 with histones H2A, H2B and DNA, but not with H3, H4 and DNA,<sup>3</sup> and recognizing the considerable evolutionary conservation of histones, it is likely that PL2-6 is binding to highly conserved histone epitopes of the nucleosome. Furthermore, an electrophoretic mobility shift assay (EMSA) of isolated Hela mononucleosomes titrated with varying amounts of PL2-6 (or 1H6) clearly demonstrated that these antibodies can bind to essentially all mononucleosomes; i.e., the epichromatin epitope is present on most (or all) nucleosomes.<sup>5</sup>

**CONTACT** Travis J. Gould  [tgould@bates.edu](mailto:tgould@bates.edu)  Department of Physics & Astronomy, 44 Campus Avenue, Lewiston, ME, USA; Donald E. Olins  [dolins@une.edu](mailto:dolins@une.edu)  Department of Pharmaceutical Sciences, College of Pharmacy, University of New England, 617 Stevens Avenue, Portland, ME, USA.  
 Supplemental data for this article can be accessed on the [publisher's website](#).

<sup>†</sup>Deceased, May 6, 2017

© 2017 Taylor & Francis

In an effort to understand the mechanism of selective epichromatin staining within the fixed and permeabilized cell (i.e., surface chromatin staining) versus the general “universal” reactivity of PL2-6 (or 1H6) with nucleosomes on chromatin strands released from swollen nuclei or with mononucleosomes by EMSA, we have performed a papain digestion of PL2-6 to generate monovalent Fab fragments. These monovalent fragments were compared to the parent bivalent PL2-6 IgG molecules employing immunostaining and biochemical methods. Unlike the bivalent molecules, immunostaining with the PL2-6 Fab fragments revealed a distinctive fine punctate (“chromomeric”) localization pattern throughout interphase nuclei and along mitotic chromosomes. In addition, Fab binding to mononucleosomes exhibited a two-step shift by EMSA analysis, suggesting two binding sites. We propose that there are two epichromatin epitopes per mononucleosome and that, from the perspective of bivalent PL2-6, these binding sites are “exposed” within the epichromatin region and “hidden” within the internal chromatin of fixed and permeabilized cells. Furthermore, we suggest, based upon peptide sequence comparisons, that the epichromatin epitope includes the nucleosome “acidic patch”<sup>6</sup>, resembling the interactions of LANA, CENPC, HMGN, and other proteins with nucleosomes.<sup>6–11</sup>

## Results

**Epichromatin Localization in Various Human Cell Lines.** Fig. 1 presents the PL2-6 immunostaining pattern of interphase and mitotic HL-60/S4, K562, GM-12878 and U2OS cells. It is clear, as described previously,<sup>1,2</sup> that the epichromatin epitope is confined to the surface chromatin underlying the interphase nucleus and to the outer surface of the cluster of mitotic chromosomes. This pattern is conserved in evolution, appearing similar in mouse, *Drosophila* and tobacco tissue culture cells<sup>1</sup>, and in the amoeboid form of *Dictyostelium discoideum* (Supplemental Figure 1).

**Super-resolution imaging of epichromatin immunostaining.** STED (stimulated emission depletion) microscopy was performed on PL2-6 stained HL-60/S4 interphase and mitotic cells. Fig. 2 presents a confocal (A) versus a STED (B) image of an interphase nucleus. The side-by-side comparison clearly illustrates the “thinner” epichromatin staining with STED

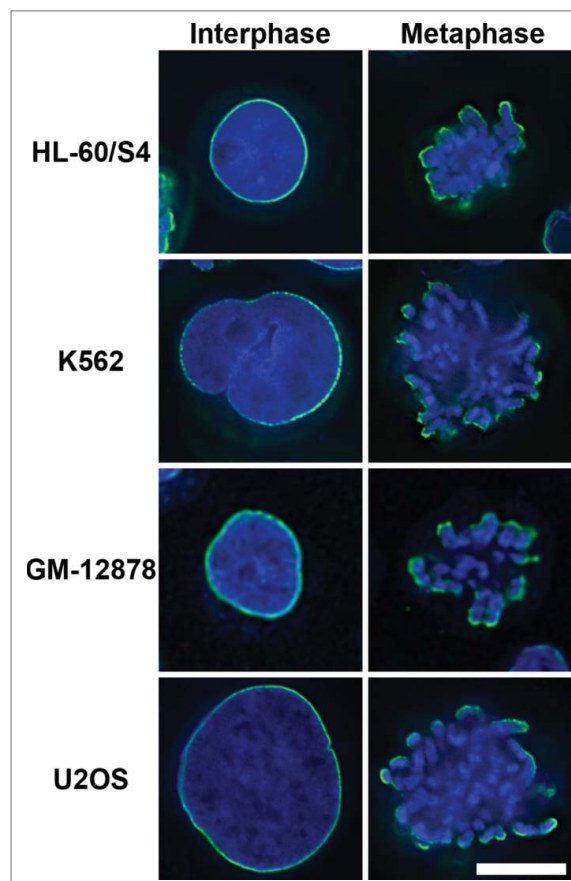


**Figure 1.** Immunostaining patterns on interphase nuclei and mitotic chromosomes from various human cell lines, employing mouse monoclonal PL2-6 antibody. The strongest immunostaining is confined to the “outer” chromatin surfaces. Images were collected using widefield microscopy followed by deconvolution on DeltaVision microscope, as described previously<sup>1,2</sup>. Magnification bar equals 10  $\mu\text{m}$ .

imaging, compared to confocal imaging. Since epichromatin appears as a “layer” of staining, we measured the layer thickness at half-maximum on line profiles perpendicular to the interphase epichromatin surface. Data from a set of confocal and a set of STED measurements of interphase epichromatin are presented in Fig. 2C and D. STED imaging yielded an  $\sim 5$ -fold increase in X/Y resolution and indicated that PL2-6 staining is largely confined to a layer of surface chromatin  $\sim 76$  nm thick. By contrast, the epichromatin region of mitotic chromosomes appears to be more “wrinkled” (Fig. 3), with ridges and valleys, compared to the “smooth” epichromatin of interphase nuclei (Fig. 2). A side-by-side comparison (confocal versus STED) of a different mitotic chromosome cluster is shown in Fig. 4. Line scans through the mitotic epichromatin yielded an average thickness of  $\sim 78$  nm,

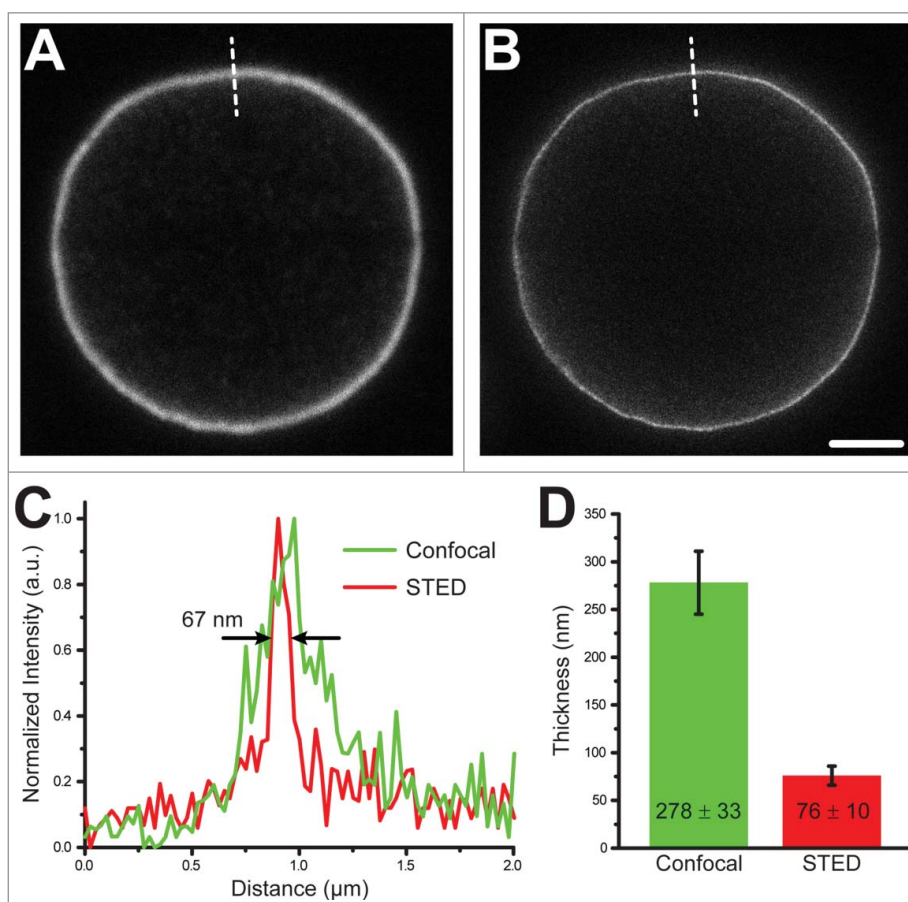


**Figure 2.** Measurement of HL-60/S4 interphase epichromatin “layer” thickness using perpendicular line profiles through confocal (A) and STED (B) microscopy images. Single line profiles are shown in (C); average values from sets of line profiles ( $N = 19$ ) are presented in (D). The magnification bar for (A, B) equals  $2\ \mu\text{m}$ . The average “layer” thickness ( $\pm$  standard deviation) for interphase epichromatin is: confocal,  $278 \pm 33\ \text{nm}$ ; STED,  $76 \pm 10\ \text{nm}$ .

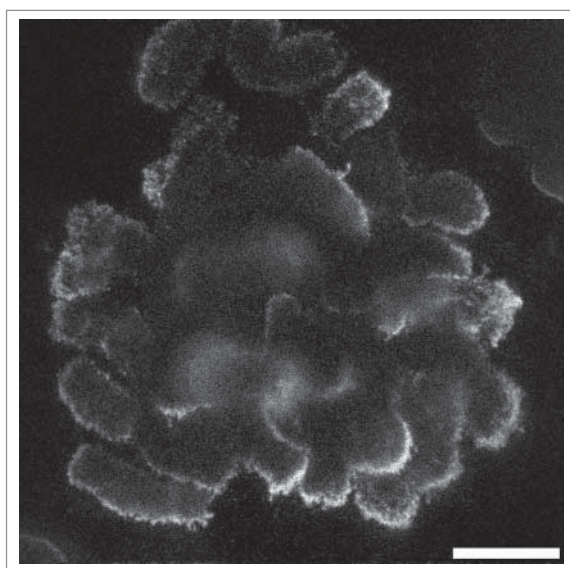


**Figure 3.** STED image of a mitotic cell stained with PL2-6. Note the “wrinkled” appearance of the mitotic epichromatin (i.e., exhibiting ridges and valleys at the chromosome boundaries), compared to the relatively “smooth” boundaries of interphase epichromatin (Fig. 2). The magnification bar equals  $5\ \mu\text{m}$ .

with a greater range of measurement values (Fig. 4C and D). The greater range in thickness measurements of mitotic epichromatin is likely due to the alternating ridges and valleys at the surface.

A recent article presented evidence that the “cell proliferation marker” Ki-67 is attached to all of the surfaces of mitotic chromosomes, where it functions as a “surfactant” to disperse the chromosome cluster.<sup>12</sup> An immediate question, consequent to this observation, is: How does Ki-67 localization relate to PL2-6 on mitotic epichromatin? Co-immunostaining with anti-Ki-67 and with PL2-6 was performed on unsynchronized HL-60/S4 cells (Fig. 5A–C). It is quite clear that Ki-67 is seen on all mitotic chromosome surfaces, whereas PL2-6 staining is primarily confined to the “outer” surfaces of the mitotic chromosome cluster. At higher magnification (Fig. 5D–F), the separate localization of Ki-67 and PL2-6 on the mitotic epichromatin was observed. “Ridges” of PL2-6 (green) were seen next to “valleys” containing Ki-67 (red).



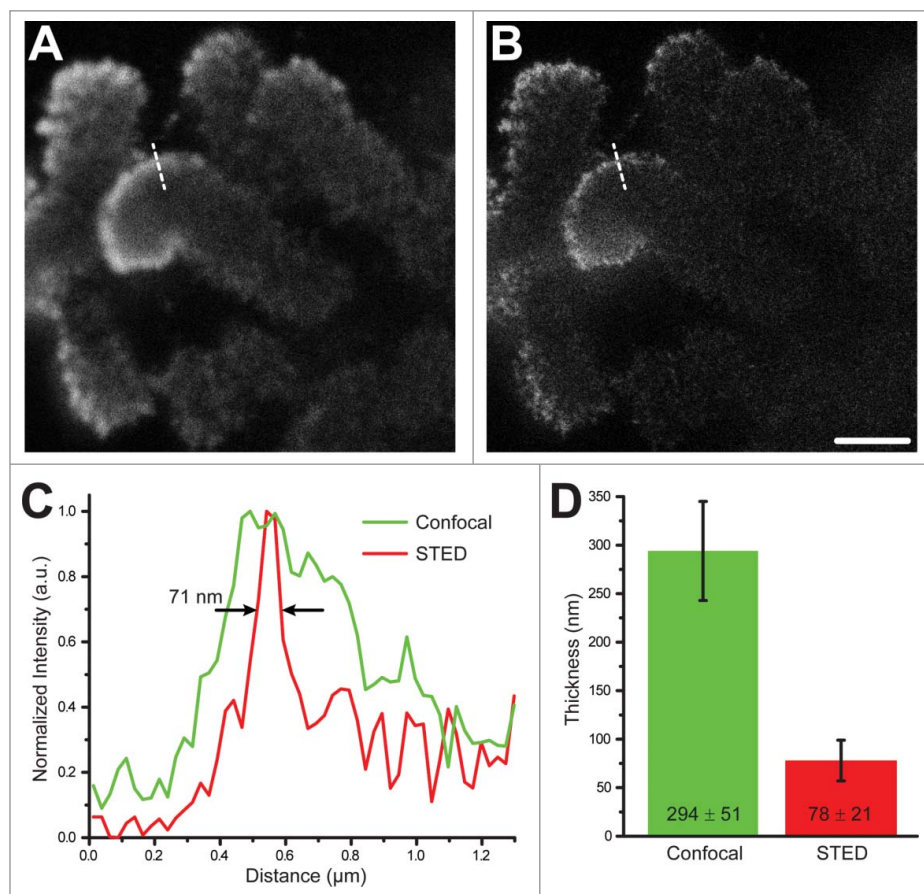


**Figure 4.** Measurement of HL-60/S4 mitotic epichromatin “layer” thickness using perpendicular line profiles through confocal (A) and STED (B) microscopy images. Single line profiles are shown in (C); average values from sets of line profiles ( $N = 52$ ) are presented in (D). The magnification bar for (A, B) equals  $2\ \mu\text{m}$ . The average “layer” thickness ( $\pm$  standard deviation) for mitotic epichromatin is: confocal,  $294 \pm 51\ \text{nm}$ ; STED,  $78 \pm 21\ \text{nm}$ .

This experiment does not permit any conclusion as to whether anti-Ki-67 and PL2-6 compete for the same epitopes; but it does appear that there is a difference between the “inner surface” and the “outer surface” (epichromatin) of a mitotic chromosome cluster.

Previously, we presented immunostaining evidence that PL2-6 (and 1H6) react with osmotically exploded chromatin from nucleated *Xenopus* erythrocytes, suggesting the concept that within internal chromatin the epichromatin epitopes are “hidden”.<sup>5</sup> To explore the level of immunostaining resolution in spread chromatin, we collected confocal and STED images of HL-60/S4 cells exploded by exposure to 0.01xPBS, prior to HCHO fixation and staining with PL2-6. An example, comparing confocal with STED is presented in Fig. 6. Measurements of “bead” diameters on the thin chromatin strands ranged from  $\sim 120$ – $175\ \text{nm}$  (pixel size was  $25\ \text{nm}$ ). Each “bead” probably represents a cluster of many nucleosomes. Immunostaining by PL2-6 of the exploded chromatin supports that the

epichromatin epitope is present (but hidden) throughout internal chromatin of the fixed intact nucleus.

Immunostaining by Monovalent Fab fragments derived from PL2-6. In an effort to discern whether antibody bivalency is essential for the surface staining pattern by PL2-6 within interphase nuclei or on mitotic chromosomes, monovalent Fab fragments were prepared using immobilized papain (Pierce Fab Micro Preparation Kit). The purified Fab fragments were analyzed by 10% SDS-PAGE under thiol reducing conditions (Supplemental Figure 2) and clearly demonstrated the fragmentation of H chains and the integrity of L chains. Numerous preparations of PL2-6 Fab always yielded the same fragmentation pattern. Immunoblot analysis of Fab fragments with total HL-60/S4 acid-extracted histones, H2A/H2B and H3/H4 subfractions (Active Motif Histone Purification Kit) indicated a strong reaction with H2A, weaker with H2B and a possible trace reactivity with H4 (Supplemental Fig. 3).

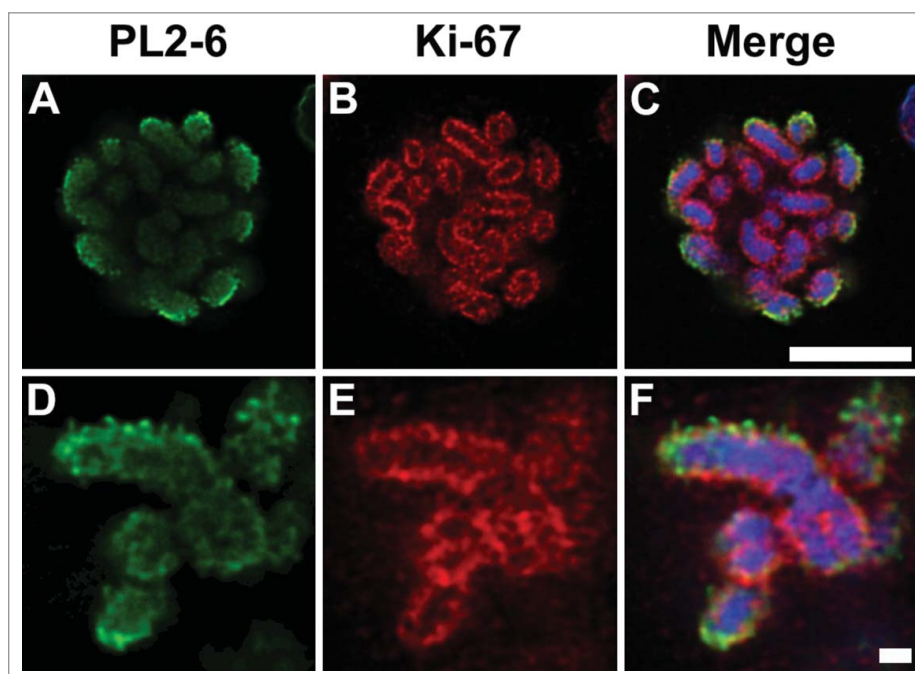


**Figure 5.** Co-immunostaining of HL-60/S4 mitotic chromosomes with PL2-6 (green), anti-Ki-67 (red) and DAPI (blue). (A-C), magnification bar equals 10  $\mu\text{m}$ . (D-F), magnification bar equals 1  $\mu\text{m}$ .

Immunostaining of undifferentiated interphase HL-60/S4 cells with the Fab fragments yielded a drastically different image than observed with the intact bivalent PL2-6 antibody. Unlike bivalent PL2-6 (Fig. 7A), monovalent Fab (Fig. 7B) revealed a “punctate” staining pattern throughout the interphase nucleus. For a comparison, simultaneously staining with bivalent rabbit anti-histone H1.5 demonstrated a similar punctate pattern, whether being paired with bivalent PL2-6 or monovalent Fab. The merged image,

combining Fab and H1.5 staining patterns indicates only “weak” co-localization between these two epitopes. Immunostaining of mitotic HL-60/S4 cells with monovalent Fab fragments revealed a punctate pattern along the chromosome arms (Fig. 7C). Bivalent anti-histone H1.5 also appeared punctate along the chromosome arms. Merged images of Fab and anti-H1.5 for several computed sections (Fig. 7D) indicate some co-localization (visualized as yellow granules), but co-localization is clearly not perfect. Fig. 8 displays

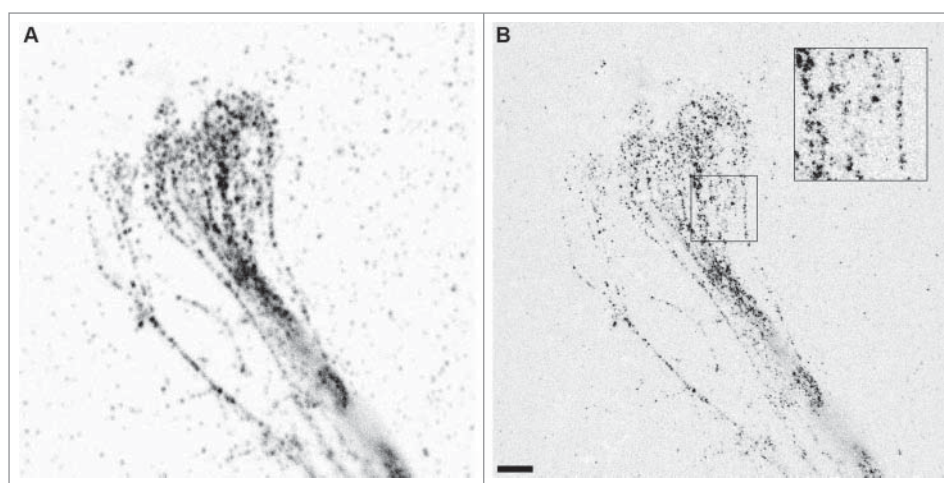


**Figure 6.** PL2-6 immunostaining of chromatin spilling out of HL-60/S4 cells, “exploded” with 0.01xPBS. Confocal (A); STED (B), with two-fold enlargement of selected field. Magnification bar equals 2  $\mu\text{m}$ .



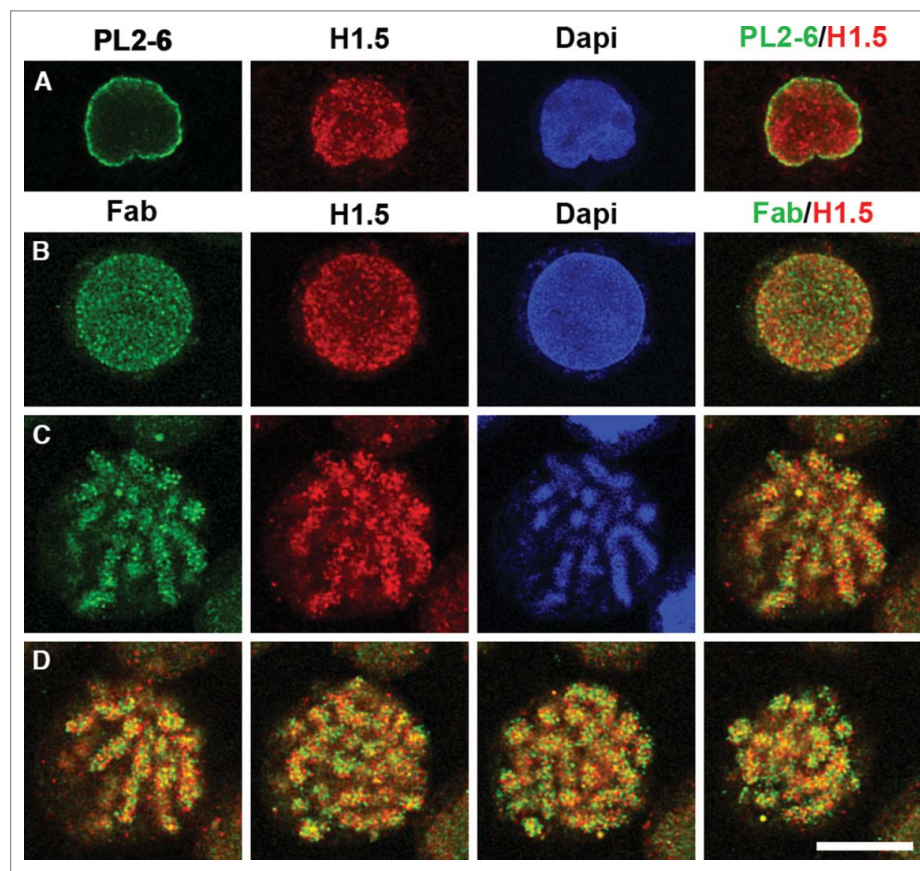


**Figure 7.** Immunostaining patterns of bivalent PL2-6 IgG and monovalent PL2-6 Fab fragments. (A) An HL-60/S4 interphase nucleus stained with bivalent PL2-6 (green) and anti-histone H1.5 (red). (B) An HL-60/S4 interphase nucleus stained with monovalent Fab (green) and anti-histone H1.5 (red). (C) A single Z-slice from a mitotic HL-60/S4 cell stained with monovalent Fab (green), anti-histone H1.5 (red) and DAPI (blue); the merged “red + green (R+G)” slice is also presented. (D) Various Z-slices of the merged R+G stack are presented. For all images, the magnification bar equals 10  $\mu\text{m}$ .

several serial sections along a mitotic chromosome arm, imaged at higher magnification, illustrating the level of partial co-localization between Fab and anti-H1.5. The identity of these  $\sim 200\text{--}300$  nm punctate structures cannot yet be defined. Because of this uncertainty, we wish to call these granular structures

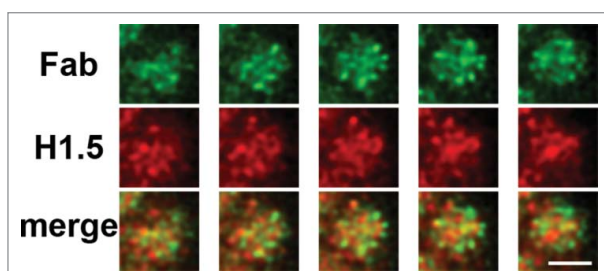


**Figure 8.** Immunostaining patterns of monovalent Fab fragments on alternate sequential Z-slices along a mitotic chromosome arm, revealing a radial “chromomeric” pattern. The top row is Fab (green); middle row, anti-histone H1.5 (red). The bottom row contains the merged “red + green (R+G)” slices. Chromomeres are  $\sim 200\text{--}300$  nm in diameter. The magnification bar equals 2  $\mu\text{m}$ .

“chromomeres”, reminiscent of the punctate structures observed along mitotic chromosome arms in the late-19<sup>th</sup> century.<sup>13,14</sup> Studying the images shown in Fig. 7 and 8, it is clear that some chromomeres are stained with Fab (green), but not with anti-H1.5 (red); some chromomeres are red, but not green. There are three major histone H1’s in HL-60/S4 cells (i.e., H1.2, H1.4 and H1.5)<sup>15</sup>; thus, it is not possible to say whether some chromomeres are devoid of histone H1, without more extensive biochemical and microscopic analyses. In addition, a careful comparison of Fab (green) with DNA (DAPI, blue) staining indicated that strong Fab is frequently seen to correspond to regions of weak DAPI staining. Likewise, strong DAPI staining regions sometimes exhibit weak Fab staining (Supplemental Fig. 4).

In summary, whereas the bivalent PL2-6 antibody immunostaining reaction is primarily confined to the surface of chromatin adjacent to the nuclear envelope or at the “outer” surface of mitotic chromosomes,

the monovalent Fab fragment localizes in punctate chromomeres, distributed throughout the interphase nucleus (excluded from nucleoli) and along mitotic chromosome arms.

Monovalent Fab fragments derived from PL2-6 bind to mononucleosomes. Previous electrophoretic mobility shift assays (EMSA) demonstrated that bivalent PL2-6 binds to “all” HeLa core mononucleosomes (at appropriate molar ratios), leading to significant electrophoretic retardation and some precipitation at the origin wells in a 1% agarose gel.<sup>5</sup> In the present study, EMSA was employed to examine the interaction of monovalent PL2-6 Fab fragments with HeLa mononucleosomes. Binding and mobility retardation was observed in these experiments, which also exhibited a reproducible buffer concentration-dependent effect on binding behavior (Fig. 9); no precipitation at the origin wells was observed. When the mixtures were examined in 1% agarose gels composed of 1xTBE buffer (Fig. 9A), the nucleosomes (normally running approximately equivalent to the 0.5 kbp DNA marker band) were retarded to a mobility slightly slower than the 1.0 kbp DNA marker band. The amount (but not mobility) of retarded mononucleosomes increased when more Fab was added; addition

of Fc fragments to mononucleosomes had no effect upon mobility. When the 1% agarose gels were run in 0.5xTBE buffer, a significant change in binding behavior was observed (Fig. 9B). At lower ratios of Fab/nucleosome, a “complex” migrated with intermediate mobility ( $\sim 0.75$  kbp DNA marker). At higher ratios, the  $\sim 0.75$  kbp band diminished in intensity and the  $>1.0$  kbp band increased in intensity, suggesting a two-step binding process. Parenthetically, in 0.5xTBE, a band was seen at less than 0.5 kbp, which also disappeared with increased ratio of Fab/nucleosome, suggesting binding of Fab to an incomplete or conformationally altered mononucleosome. Examining this buffer concentration-dependent effect upon Fab/nucleosome interaction and mobility, we were reminded of earlier observations on the binding of HMGN1 and 2 (previously called HMG-14/17) to mononucleosomes.<sup>16,17</sup> At that time, we demonstrated that each of these proteins bound to two identical sites on the core mononucleosome, showing a similar “cooperative” binding pattern in higher ionic strength buffer versus a stepwise “non-cooperative” binding in lower ionic strength. By analogy to the interaction of HMGN1 and 2 to the core mononucleosome, we suggest that the Fab binding behavior (Fig. 9) implies two binding sites (epitopes) per nucleosome (presumably symmetrical around the nucleosome dyad axis).

Analytical ultracentrifugation studies were performed on Fab/mononucleosome complexes in 1xTBE buffer (Fig. 10, at an approximate molar ratio of 5/1; see EMSA image, Fig. 10C). Fig. 10A presents the results of a sedimentation velocity experiment, depicted as a distribution of sedimentation coefficients. At the peak of the distribution, the core mononucleosome exhibited an  $s_{20,w}$  equal to 10.2 S; the Fab/mononucleosome complex exhibited an  $s_{20,w}$  equal to 12.6 S, with a small amount of apparently non-complexed mononucleosomes. Fig. 10B presents the results of a sedimentation equilibrium experiment, allowing estimation of the apparent molecular mass ( $M_{app}$ ) for the mononucleosome ( $\sim 197$  kg/mol) and for the Fab/mononucleosome complex ( $\sim 281$  kg/mol). The complex is slightly less than the expected  $M_{app}$  for a nucleosome plus two Fab fragments ( $\sim 300$  kg/mol), possibly reflecting a small amount of “free” mononucleosome.

In summary, the combination of EMSA and analytical ultracentrifugation methods are consistent with the formation of a complex consisting of 2 Fab

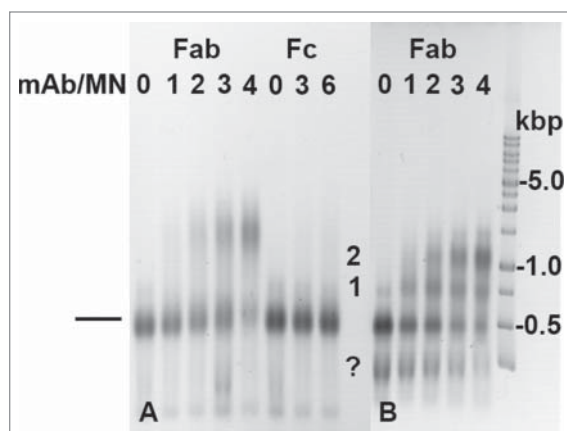


**Figure 9.** Electrophoretic Mobility Shift Assay (EMSA) demonstrating the binding of monovalent Fab fragments to HeLa mononucleosomes (MN). (A) Titration in 1xTBE with an increasing input molar ratio of Fab/mononucleosomes (mAb/MN) demonstrating that at a sufficiently high ratio, almost all MN exhibit mobility retardation; at comparable molar ratios, Fc fragments have no effect. (B) Titration in 0.5xTBE with an increasing input molar ratio (mAb/MN). Binding and electrophoresis in 1xTBE buffer produces a “cooperative” binding pattern with two migrating bands; at lower ionic strength (0.5xTBE) a “non-cooperative” binding pattern is observed (i.e., a complex with intermediate retarded mobility, presumably binding one Fab, analogous to HMGN binding<sup>16,17</sup>). Black bar denotes the position of the intact MN; “?”, the position of incomplete or conformationally altered MN.

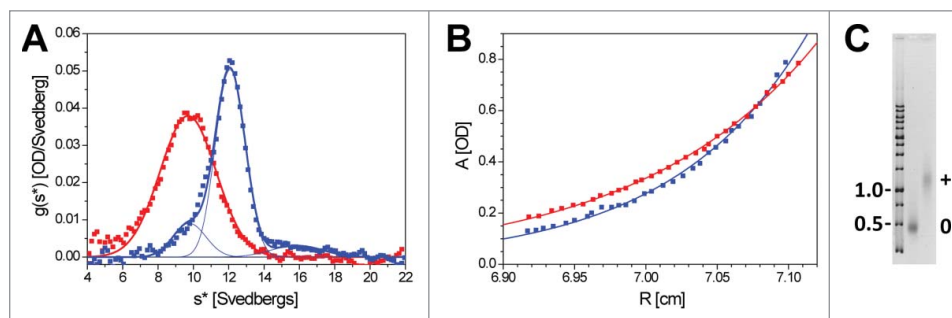


**Figure 10.** Analytical ultracentrifugation of Fab/mononucleosomes (MN) complexes in 1xTBE buffer. (A) Distribution of the sedimentation coefficient ( $s_{20,w}$ ) for HeLa mononucleosomes (red, -Fab) and for a 5/1 molar ratio (blue, +Fab). The peak values were: -Fab,  $s_{20,w} = 10.2$  S; +Fab,  $s_{20,w} = 12.6$  S. The distributions were fitted with Gaussian curves. (B) Equilibrium sedimentation determination of apparent molecular weights ( $M_{app}$ ) for HeLa mononucleosomes (red, -Fab) and for a 5/1 molar ratio (blue, +Fab). The measured values were: -Fab,  $M_{app} = 197$  kg/mol; +Fab,  $M_{app} = 281$  kg/mol. (C) EMSA in 1xTBE of the samples examined by analytical ultracentrifugation. DNA markers: 0.5 and 1.0 kbp. Samples: 0, MN; +, MN + Fab.

fragments bound to a single mononucleosome, which is stable at moderate ionic strength (e.g., 1xTBE) in the presence of a molar excess of Fab fragments.

**The nucleosome acidic patch: a candidate epichromatin epitope.** Mouse monoclonal antibody PL2-6 and its Fab fragment are clearly anti-nucleosome antibodies. From the previous data, it seems likely that there are two binding sites on each (and all) nucleosomes. The peptide sequences of the variable regions of the PL2-6 H and L chains have been determined<sup>3</sup> and deposited into the IMGT database (Hv: X60334; Lv: X60341). Of particular interest is Hv3 (i.e., the H chain third complementarity-determining region, or “variable region”). The peptide sequence of PL2-6 Hv3 resembles comparable regions of anti-DNA antibodies, even though PL2-6 does not bind to DNA.<sup>3</sup> Of particular interest, one peptide motif within PL2-6 Hv3 (..RLRS..) resembles peptide motifs of proteins that have been shown to bind to the nucleosome “acidic patch” (Fig. 11A).

The acidic patch<sup>6,8,9</sup> is structurally defined by the presence of 8 acidic amino acids (6 from histone H2A; 2 from H2B) at the junction of histones H2A and H2B. There are two acidic patches per nucleosome, symmetrically related by the nucleosome dyad axis. A number of diverse proteins have been shown by X-ray crystallography, NMR and model building to bind to the acidic patch. No single peptide chain conformation within the various binding proteins satisfies the conditions for maximum residue contact; different proteins exhibit different peptide conformations in their interaction with the acidic patch (see Fig. 4<sup>6</sup> and Fig. 2<sup>9</sup>, for representations of the diverse peptide folding on the acidic patch). It seems reasonable to suggest

that PL2-6 Hv3 can resemble LANA, CENPC or other proteins in a similar interaction with the acidic patch. PL2-6 has the additional complexity (and/or advantage?) of having two peptide chains (H and L) defining the antibody binding site. It is not possible to decide which of the PL2-6 Hv3 motif residues (..RLRS..) is most critical for interaction specificity; however, by analogy with LANA, one might predict that the second arginine interacts with a triad of H2A acidic residues (i.e., E61, D90 and E92) by forming salt bridges.<sup>6</sup> It is of interest that a “sister” monoclonal

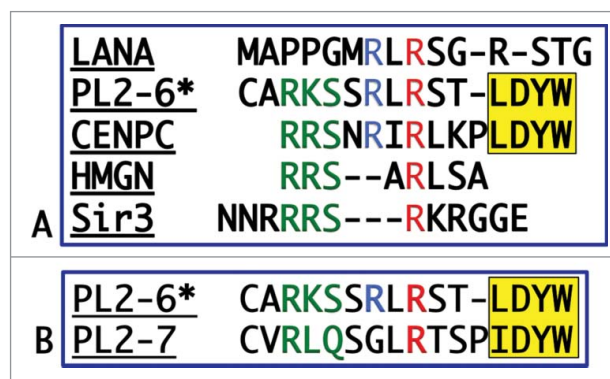


**Figure 11.** Peptide sequence comparisons. (A) The PL2-6 heavy chain variable region 3 (Hv3) compared to various nucleosome acidic patch binding proteins. The second arginine (red R) in the LANA (...RLRS...) sequence forms salt bridges with H2A E61, D90 and E92.<sup>6</sup> The yellow (...LDYW...) motif is a common hydrophobic structural feature of many Hv3 regions. (B) Comparison of the Hv3 regions of PL2-6 and PL2-7. Both antibodies are from the same mouse spleen and both show preferential binding to H2A/H2B/DNA by ELISA.<sup>3</sup> However, PL2-6 stains epichromatin in the fixed intact nucleus, whereas PL2-7 stains throughout the interphase nucleus.<sup>2</sup> This may indicate the importance of the first arginine (blue R) in the (...RLRS...) sequence. Other similarities and differences are seen in the highlighted green sequences.



anti-nucleosome bivalent antibody, PL2-7 (from the same mouse spleen as PL2-6 and which gives similar ELISA results [i.e., maximal binding to H2A/H2B/DNA]<sup>3</sup>, but a different immunostaining pattern [i.e., punctate staining throughout the interphase nucleus])<sup>2</sup>, exhibits a changed residue in the motif (..RLRS.. becomes ..GLRT..) (Fig. 11B). The first arginine in the LANA motif forms a salt bridge with H2B E110.<sup>6</sup> This amino acid residue difference supports the argument that the epichromatin immunostaining pattern depends upon the integrity of the (..RLRS..) motif within PL2-6 Hv3 region. Although mAb 1H6 strongly resembles PL2-6 in terms of immunostaining of fixed cells and immunoblotting against acid extracted histones<sup>2</sup>, also with respect to EMSA and ChIP-Seq results<sup>5</sup>, due to the absence of Hv and Lv peptide sequence data, it is not yet possible to argue that 1H6 may have the nucleosome acidic patch as a candidate epitope.

## Discussion

The present study is an attempt to define the properties of epichromatin (the surface of chromatin adjacent to the interphase nuclear envelope and the “outer” surface of mitotic chromosomes), to infer the characteristics of the epichromatin epitope and to suggest a possible functional significance for epichromatin. So far, epichromatin can only be identified by immunostaining with two mouse monoclonal antibodies of different origin (PL2-6 and 1H6).<sup>1,2</sup> These identifying antibodies yield similar immunostaining images with cells of very diverse evolutionary origin (i.e., human, mouse, *Xenopus*, *Drosophila*, *Caenorhabditis*, tobacco, *Arabidopsis* and *Dictyostelium*).<sup>1,2,5</sup> It is very unlikely that common DNA sequences across such a diverse range of species are responsible for this common epitope. It is more likely that common nucleosome features, which are highly conserved by evolution, form the basis of the similar immunostaining patterns.

Based upon a comparison between confocal and STED imaging, it appears that the epichromatin epitope is confined to a thin layer ( $\sim 76$  nm;  $\sigma$ ,  $\pm 10$  nm) adjacent to the interphase nuclear envelope. The immunostaining reaction with mitotic chromosome surfaces yields a comparable ( $\sim 78$  nm) thickness with greater variation ( $\sigma$ ,  $\pm 21$  nm). Present data suggests that this variable thickness at the surface of mitotic

chromosomes is a reflection of its “wrinkled” surface (i.e., displaying ridges and valleys), compared to epichromatin adjacent to the interphase nuclear envelope (compare Figs. 2 and 4). A recent publication describes the localization and functional significance of Ki-67 bound to the surface of mitotic chromosomes<sup>12</sup>. Ki-67 acts as a surfactant, preventing the cluster of mitotic chromosomes from collapsing on itself, which results in defective mitotic chromosome separation. In the present study, we show (Fig. 5) that Ki-67 binds to all mitotic chromosome surfaces, including the “outer” epichromatin surface, which is highlighted by PL2-6 binding. Indeed, as demonstrated by co-immunostaining with anti-Ki-67 and PL2-6, Ki-67 appears to be interspersed between PL2-6 staining (i.e., PL2-6 stains the “ridges”, Ki-67 is often localized to the “valleys” of the mitotic epichromatin).

It appears that the epichromatin epitope is present on all (or most) nucleosomes, as detected by immunostaining hypo-osmotically “exploded” cells with chromatin strands spilling out (Fig. 6). In addition, both bivalent PL2-6<sup>5</sup> and (papain-derived) monovalent PL2-6 Fab fragments bind to “all” mononucleosomes, as assayed by electrophoretic mobility shift assay (EMSA) (Fig. 9). The simplest interpretation for the confinement of the epichromatin epitope to the surface chromatin of fixed and permeabilized cells versus the presence of the epitope on “all” nucleosomes is, that most epitopes are “hidden” within the interior chromatin; whereas, many epitopes remain “exposed” at the chromatin surface. This distinction between “hidden” and “exposed” epitopes is especially clear, when immunostaining with the bivalent PL2-6 or 1H6 antibodies.

Indeed, immunostaining with monovalent PL2-6 Fab fragments yields a surprisingly different picture, compared to what is observed with the bivalent form of PL2-6. The Fab fragments generate punctate staining ( $\sim 200$ – $300$  nm diameter) throughout the interphase nucleus (excluding nucleolar regions) and along mitotic chromosome arms. Because we do not know the structural basis of the punctate staining, we refer to them as “chromomeres”, reminiscent of late 19th Century classical microscopic observations.<sup>13,14</sup> A similar chromomeric pattern (with some degree of colocalization) was observed during co-immunostaining combining monovalent Fab with bivalent antibodies against histone H1.5. Bivalent anti-H1.5 yields a similar punctate pattern during immunostaining of

chromatin, as is observed with monovalent PL2-6 Fab fragments. In principle, either bivalent or monovalent antibodies can experience “hidden” or “exposed” epitopes.

It is not clear what level of chromatin structure is represented in the chromomeric pattern of Fab staining. The human diploid genome consists of  $\sim 6 \times 10^9$  bp (actually, HL-60/S4 is hypodiploid<sup>18</sup>). Assuming 200 bp/nucleosome, this calculates to  $\sim 3 \times 10^7$  nucleosomes per diploid nucleus. Assuming that TADs (topologically associating domains or megabase “globules”)<sup>19,20</sup> contain  $\sim 10^6$  bp DNA, yields an estimate of  $\sim 6,000$  TADs per diploid nucleus. We have estimated the total numbers of Fab chromomeres within diploid interphase nuclei and within tetraploid metaphase groups of mitotic chromosomes, examining the total number of “spots” (corrected to diploid) in the stack of Z-slices and varying the “threshold” for each slice. The total number of spots/diploid as a function of threshold is shown in Supplemental Figure 5. A video of an interphase nuclear stack stained with Fab (at 20% threshold, Supplemental Video 1) displays  $\sim 2791$  chromomeres/diploid. A video of a mitotic stack at 20% threshold (Supplemental Video 2 [the identical stack as shown in Fig. 7C and D]) displays  $\sim 1150$  chromomeres/diploid. Clearly, the interphase and mitotic chromomeres cannot correspond to nucleosomes; more likely, we are visualizing higher-order nucleosome clusters (possibly TADs, but they are believed to be absent from mitotic chromosomes, employing Hi-C technology<sup>21</sup>). At any threshold level, the total number of mitotic chromomeres (corrected to diploid) is considerably less than the total diploid number of interphase chromomeres. Conceivably, this reduction in apparent chromomeres during mitosis could be due to decreased epitope “exposure”, to dissolution of the chromomere structure or to consolidation of chromomeres.

The conception of chromatin as particulate structures ( $\sim 0.5$ – $1.0$  Mbp DNA) within the hierarchy of chromatin higher-order organization is not a new idea. This conception is also intimately connected to models of DNA replication foci.<sup>22–24</sup> In a recent super-resolution microscopy study of chromatin dynamics within live interphase cells, evidence was presented that chromatin is condensed into clusters of  $\sim 600$ – $1000$  nucleosomes (“compact domains”), which exhibit coherent movement.<sup>25</sup> The diameter of these compact domains in live cells is  $\sim 220$  nm, which

shrinks to  $\sim 160$  nm following formaldehyde fixation. Clusters of nucleosomes are also seen in mitotic chromosomes, which shrink to a diameter of  $\sim 140$  nm following fixation. It seems very likely that our “chromomeres” are equivalent to the reported “compact domains”. If so, this correspondence suggests that compact domains may have an enrichment of “exposed” nucleosome acidic patches on their surfaces and might be stabilized as a cluster (in part) by H1 histones.

The preparation of PL2-6 Fab fragments permitted EMSA and hydrodynamic ultracentrifugation characterization of the Fab-monomonucleosome complex, supporting the conclusion that there are two epichromatin epitopes per nucleosome. A comparison of peptide binding motifs to the nucleosome acidic patch (Fig. 11A), underscores the similarity of the PL2-6 Hv3 loop<sup>3</sup> to established acidic patch binding proteins, LANA, CENPC, HMGN and Sir3.<sup>6–8</sup> A critical arginine in LANA (R9, the second R in ..RLRS..) has been shown to participate in salt bridges with histone H2A E61, D90 and E92. The other arginine of the binding motif (R7) shows a salt bridge with H2B E110. These interactions suggest an analogous structural model for the PL2-6 Hv3 loop interacting with the nucleosome acidic patch.

A difficulty with making a strict analogy between PL2-6 Hv3 and the acidic patch binding proteins is that PL2-6 is composed of both H and L chains; whereas, the other acidic patch binding proteins are binding as single peptide chains. There exists the distinct possibility that the L chain can modulate the binding specificity and interaction strength of PL2-6 Hv3 with the epichromatin epitope. In fact, this effect of L chain modulation has been clearly established with anti-DNA antibodies. It has been known for many years that the Hv3 region of anti-DNA antibodies displays an enrichment of arginine residues.<sup>3,26–28</sup> In one example of an anti-DNA antibody (A52), with an Hv3 loop sequence that strongly resembles PL2-6 (Supplemental Fig. 6), the Fab fragment has been crystallized and the 3D structure solved to  $1.62 \text{ \AA}$ .<sup>29</sup> By analogy to the crystal structure of A52 Fab, Fig. 12 presents a speculative model of the PL2-6 Fab fragment (model generated by Dr. Robyn Stanfield, The Scripps Research Institute, La Jolla, CA), highlighting three arginines on the PL2-6 Hv3 loop and one arginine on the L chain. It is now clear that certain “editor” L chains can “diminish or veto” the anti-DNA affinity for certain antibodies that have a high arginine content in



the Hv3 region.<sup>30</sup> PL2-6 shows no binding to DNA (single- or double-stranded).<sup>3</sup> It is conceivable that PL2-6 may be a combination of anti-DNA H chains, modified by the L chains to prefer to bind to the nucleosome acidic patch. In fact, a different anti-DNA antibody (3H9) has been demonstrated to bind to chromatin, possesses an essential arginine (R96) in the Hv2 loop, and has been suggested to bind to the nucleosome acidic patch.<sup>31</sup> Furthermore, 3H9 has been demonstrated to bind to phosphatidylserine (with a loss of anti-DNA activity) following conversion of an Hv arginine to a glycine.<sup>32,33</sup> This is of interest, since we have reported that an anti-phosphatidylserine antibody (1H6) binds to mononucleosomes and stains epichromatin.<sup>2</sup> It is clear that Hv arginine content and positions and “editor” L chain properties can modulate the binding properties of anti-DNA, anti-chromatin and anti-phospholipid antibodies in complex ways. Unfortunately, no amino acid sequence data is currently available for mAb 1H6, preventing sequence comparisons to PL2-6 and other antibodies of interest.

Assuming that the epichromatin epitope includes the nucleosome acidic patch, one can speculate on the possible differences between the epitope “hidden” and “exposed” states. Since there is evidence that the N-terminal tail of histone H4 (from an adjacent nucleosome) can interact with the acidic patch<sup>6</sup>, and interphase epichromatin is at the surface (i.e., between internal chromatin and the inner nuclear membrane), the amount and distribution of H4 tails should be quite different on both sides of epichromatin. In addition, molecular simulation studies indicate that acetylation of a lysine (K16) on the N-terminal tail of histone H4 should weaken interactions between H4K16 and the acidic patch.<sup>34</sup> It is not known if H4K16Ac is enriched within the epichromatin region. Besides the histone H4 tail, other nuclear acidic patch binding proteins (e.g., HMGN1 and 2) may have a differential nuclear distribution which might also be preserved by formaldehyde, maintaining the distinction between the “hidden” and “exposed” epitope states.

Why does the bivalent PL2-6 antibody immunostain so differently than the papain-derived monovalent PL2-6 Fab fragment? Conceptually, there are, at least two antigenic structural parameters that might influence the apparent intensity of the immunostaining reaction with bivalent antibodies, the concentration of the epitope and the geometric arrangement of the epitopes. Monovalent Fab fragments should be less sensitive than bivalent PL2-6 to the geometric

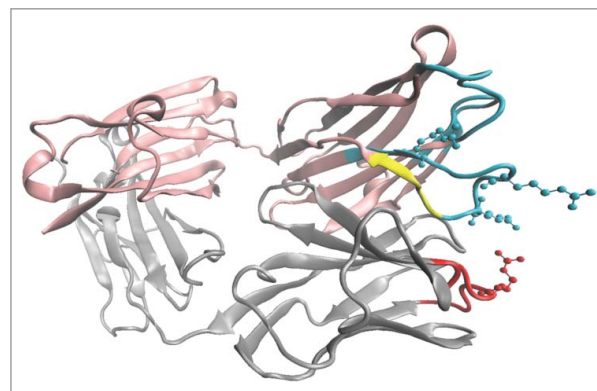


**Figure 12.** Model of PL2-6 Fab fragment constructed by Dr. Robyn Stanfield (The Scripps Research Institute). The Hv3 region (blue) displays three R residues; the Lv1 region (red), one R residue in the antibody binding site. The hydrophobic yellow (...LDYW...) motif is also indicated.

arrangement. The unique importance of epitope geometric arrangement to the bivalent antibody involves the concept of “avidity”, which is defined as the “ability to simultaneously bind two physically linked antigens...by using the two identical combining sites located at the tips of their Fab (antigen-binding fragments) arms”.<sup>35</sup> Avidity is essentially the association constant of the bivalent antibody. Modeling studies<sup>36</sup> have clearly shown that avidity is a function of the 2D planar epitope “surface concentration” ( $\sigma$ ). As  $\sigma$  increases, “bivalent binding dominates because there are ample opportunities for the second Fab to bind through the fast exploration of a reduced volume. Concomitantly, the number of monovalent bound antibodies decreases as  $\sigma$  increases.”<sup>36</sup> We suggest that the epichromatin epitope (i.e., presumably, the acidic patch) is exposed at a high surface concentration and with “acceptable” geometric arrangement, which collectively favor the binding of bivalent PL2-6. Internal chromatin is assumed to consist of hidden epitopes and scattered exposed epitopes, which are sterically more favorable to monovalent Fab binding and less favorable to the bivalent PL2-6. Acceptable geometric arrangements of the epichromatin epitope are defined by the structural parameters of the bivalent IgG molecule (i.e., distance between the antibody binding sites on one IgG, ~15 nm; flexible and rotatable joints between the two Fab regions and the Fc region; distance between the joints and the Fab binding site, ~7 nm), and by those of the nucleosome and the orientations of the acidic patch. Furthermore, the IgG molecule has a dyad axis relating the orientation of

the two binding sites, an additional constraint upon the orientations of suitable epitopes. Consequently, we propose that difference in epitope geometric arrangements is a major factor in confining epichromatin immunostaining to the surface of chromatin.

In a previous publication,<sup>5</sup> we demonstrated that ChIP-enriched epichromatin from human HL-60/S4 cells (undifferentiated, granulocytic and macrophage forms) has unusual DNA sequence properties: 1) only ~4% of the genome is enriched. 2) retrotransposon Alu is enriched ~10 fold above the average genome density. 3) epichromatin enrichment is discontinuous with chromosome-specific distributions. We are presently lacking comparative enrichment studies from other cell types and/or different species. Since Alu is restricted to primates, enrichment studies in more distant species than primates, cannot possibly yield the same DNA sequence properties for epichromatin. Even so, essentially identical immunostaining patterns with PL2-6 are obtained with a large variety of cell types. We must conclude that exposure of the epichromatin epitope adjacent to the cell nucleus or at the surface of mitotic chromosomes is not a direct consequence of the underlying DNA sequence, but rather, to the exposure and geometric arrangement of nucleosome (acidic patches) within the 3D nuclear or mitotic chromosomal architecture.

Finally, we speculate on the adaptive advantage of maintaining nucleosomes with “exposed” chemical properties (e.g., acidic peptide residues) on chromosomal surfaces (in particular, mitotic epichromatin). The “wrinkled” mitotic epichromatin may be a mechanism for increasing the density of “exposed” chromatin epitopes. We suggest that “exposed mitotic nucleosomal surfaces” might be attractive to inner nuclear membrane proteins and their adaptors (e.g., LBR, LAP2 $\beta$ , Emerin, MAN1 [BANF, a LEM adaptor<sup>37</sup>]) or to membrane phospholipids, which could be attracted to unaffiliated histone basic tails that extend out from the surface nucleosomes. These potential interactions might facilitate post-mitotic nuclear envelope reformation.<sup>38,39</sup> In the HL-60/S4 cell system, epichromatin has a high nucleosome density, intersects regions of high DNase I sensitivity and exhibits a paucity of many histone post-translational modifications.<sup>5,40</sup> Perhaps mitotic epichromatin presents an “open” and less modified chromatin structure facing the telophase-adhering endoplasmic reticulum, facilitating rapid membrane attachment and growth.

## Dedication

This article is dedicated to the memory of Jörg Langowski, who died on May 6, 2017. Jörg was enthusiastic about science, was generous, stimulating and critical, fought for honesty, and was a true friend. He is greatly missed.

## Methods

Cells, Antibodies and Papain-digestion. Cultivation of HL-60/S4 has been described previously<sup>1</sup>. K562 and U2OS cells were maintained as described by ATTC (Manassas, VA); GM12878, as described by the Coriell Institute for Medical Research (Camden, NJ). Mouse monoclonal PL2-6 was originally developed and tested in 1992.<sup>3</sup> The initial use of PL2-6 to identify epichromatin was published later.<sup>1</sup> PL2-6 was employed at a 1:100 dilution. Papain digestion of mAb PL2-6 was achieved with a Pierce Fab Micro Preparation Kit (Thermo Scientific #44685). The monovalent Fab fragments were employed at a 1:25-1:50 dilution. For confocal imaging of PL2-6 and Fab, an Alexa 488 donkey anti-mouse IgG (H+L) antibody was used at a 1:1000 dilution. For STED microscopy of mAb PL2-6, we employed, as a secondary antibody, Abberior STAR 488 goat anti-mouse IgG at a dilution of 1:100. Rabbit anti-histone H1.5 was purchased from Abcam (ab18208) and used at 1:500; rabbit anti-Ki-67 (ab15580) was used at 1:1000. In these cases, an Alexa 568 goat anti-rabbit IgG antibody was used at a 1:1000 dilution.

Nucleosomes. HeLa cells were maintained in suspension culture in RPMI 1640 medium without phenol red, supplemented with 10% fetal calf serum. Isolation of nuclei and fractionation of chromatin into mono- and oligonucleosomes was performed as previously described<sup>41</sup>. Fractions containing primarily mononucleosomes were dialysed overnight against 20 mM Tris, 50 mM NaCl (pH 7.4) and concentrated in Centricon cartridges (Centricon, MA). SDS and native polyacrylamide gel analysis were used to determine whether the mononucleosomes were truncated to core particles, containing DNA fragments < 150 base pairs and the four core histones in equimolar proportion. Linker histones or non-histone proteins were not detectable within the samples.

Electrophoretic Mobility Shift Assay (EMSA). Nucleosomes and their complexes were run in 1% agarose gel with 10 V/cm electric field. We used a

modified 1xTBE buffer (31 mM Tris, 194 mM boric acid, 1.88 mM EDTA, pH 7.5) in which the nucleosomes are stable. After ~90 min of electrophoresis, the gels were stained with ethidium bromide to visualize DNA containing bands by fluorescence. Markers including both 100bp and 1000 bp DNA ladders were employed for comparison.

**Analytical ultracentrifugation.** Experiments were conducted with a Beckman analytical ultracentrifuge (Optima XLA), equipped with an ultraviolet absorption optical system. Sedimentation velocity experiments were carried out in double-sector charcoal-Epon cells. Scans were recorded at 260 nm for mononucleosomes and their complexes. Data were analyzed with the DCDT program to obtain the sedimentation and diffusion coefficients, molecular mass and  $g(s^*)$ . Sedimentation equilibrium runs were carried out in six-channel charcoal-Epon cells. The data were analyzed with the program Winnonlin V1.035 ([ftp://alpha.bbri.org/rasmb/spinms\\_dos/uconn\\_uaf](ftp://alpha.bbri.org/rasmb/spinms_dos/uconn_uaf)).

**Widefield Deconvolution and Confocal microscopy.** Widefield deconvolution microscopy was accomplished with a DeltaVision microscope, as described previously<sup>1,2</sup>. Confocal imaging was performed on a Leica SP8 microscope. All images were collected as stacks, where each slice was  $1024 \times 1024$  pixels. Z steps were  $0.25 \mu\text{m}$ . Confocal stacks were deconvolved with Autoquant X3 using an adaptive psf (point spread function). Figures were prepared in Adobe Photoshop.

**STED microscopy.** STED microscopy<sup>42</sup> was performed on a home-built system (constructed by TJ Gould at Bates College) featuring 592 nm continuous wave depletion (MPB Communications) and 500 nm pulsed excitation (PicoQuant) lasers. The laser lines were combined using dichroic mirrors, passed through a commercial scan head (Yanus IV, FEI) and focused into the sample by a 100X/1.4NA oil immersion objective lens (Olympus) mounted in a commercial microscope stand (IX71, Olympus). Samples were mounted onto a z piezo stage (Mad City Labs) for axial positioning. A spatial light modulator (SLM; Hamamatsu) in the depletion beam path was imaged into the back focal plane of the objective lens to provide phase modulation for shaping the depletion focus. A helical phase ramp was applied to generate the standard toroidal depletion focus for lateral resolution enhancement in STED microscopy. Additionally, the SLM was used to remove residual system

aberrations using the aberration correction routines previously described<sup>43</sup>, and for maintaining alignment between the excitation and depletion foci using the auto-alignment procedure.<sup>44</sup> Half- and quarter-wave plates were used to generate circular polarization for both beams at the sample. Signal from the sample was collected by the objective lens, descanned, separated from the lasers using dichroic mirrors, bandpass-filtered (540/50, Chroma), and focused onto a  $62.5 \mu\text{m}$  core diameter ( $\sim 0.8$  Airy units) multimode fiber (Thorlabs) connected to a single-photon counting module (ARQ-13-FC, Excelitas). The detected signal was time-gated for additional resolution enhancement<sup>45</sup> using custom designed gating electronics (Opsero Electronic Design) with a software programmable detection window of 8 ns, delayed 1–2 ns with respect to the excitation pulse. Hardware control and data acquisition was performed using custom-written software in Labview (National Instruments). Images were acquired at a scan rate of 2000 lines/s, a pixel size of 25 nm, and with either 80–100 (STED mode) or 40–50 (confocal mode) line accumulations. Laser powers at the back focal plane of the objective lens were  $\sim 160$  mW and  $\sim 10 \mu\text{W}$  for depletion and excitation, respectively. For a given field of view, STED and then confocal images were acquired sequentially for comparison.

**Measuring epichromatin thickness.** The thickness of epichromatin rim-staining was measured as the full-width half-maximum (FWHM) of intensity line profiles. Using custom software written in Matlab (Mathworks), line profiles across the epichromatin “rim” signal were background subtracted using a nearest neighbor spline interpolation and then fitted to a one-dimensional Lorentzian (STED images) or Gaussian (confocal images) to determine the FWHM.

**Image Segmentation for Counting Fab Spots.** Confocal z-stacks of Fab were deconvolved (using AutoQuant X3 software) and analyzed using watershed segmentation to determine the number of observed Fab spots in interphase nuclei and mitotic chromosomes. Using custom software written in Matlab, deconvolved z-stacks were first top hat filtered using an ellipsoidal structuring element (6 pixel radius in X/Y, 2 pixel radius in Z). Pixel values were normalized to the maximum signal in each z-slice and contrast was adjusted using the contrast-limited adaptive histogram equalization function. Each stack was subsequently binarized by thresholding each slice according to a

percentage of the maximum intensity in that frame and area-opened to remove small ( $< 10$  pixel area) spurious regions. Segmentation was then performed as a function of this percentage as follows. The distance transform was computed of the logical complement of the binarized stack. By computing the watershed transform of the negative of this distance transform, bright objects in the original stack (i.e. Fab spots) are identified as “catchment basins” separated by “watershed lines”. The final stage of segmentation consisted of computing the logical AND of the binarized stack and 3D watershed lines. Finally, the number of Fab spots was determined by finding the number of three-dimensionally connected regions (with at least a 6-connected neighborhood) in the segmented stack. All processing steps were performed using the functions provided by Matlab’s Image Processing Toolbox.

### Disclosure of potential conflicts of interest

No potential conflict of interest were disclosed.



### Acknowledgments

The authors thank Nathan Poulin for STED imaging assistance, Edward Allgeyer for Labview assistance, and Peter Beach for machining services. The authors express their appreciation to numerous individuals, who have called our attention to nucleosome acidic patch binding proteins, especially Maria Hondele, Ruihan Zhang, Yawen Bai, Grisha Armeev, Alexey Shaytan and Anna Panchenko. The model in Fig. 12 was constructed by Robyn Stanfield and rendered by Elizabeth Whitmore. The authors also thank Igor Prudovsky for use of the Leica SP8. Heike Ziegler and Wolfgang Nellen kindly provided *Dictyostelium discoideum* cells for immunostaining. ALO and DEO express their appreciation to the University of New England and to the German Cancer Research Center for hosting us in their laboratories.

### Funding

This work was supported in part by an Institutional Development Award (IDeA) from the National Institute of General Medical Sciences of the National Institutes of Health under grant number P20GM0103423 (TJG).

### ORCID

Jörg Langowski  <http://orcid.org/0000-0001-8600-0666>  
Donald E. Olins  <http://orcid.org/0000-0002-6088-0842>

### References

- [1] Olins AL, Langhans M, Monestier M, Schlotterer A, Robinson DG, Viotti C, Zentgraf H, Zwerger M, Olins DE. An epichromatin epitope: persistence in the cell cycle and conservation in evolution. *Nucleus* (Austin, Tex). 2011;2:47-60. PMID:21647299
- [2] Prudovsky I, Vary CP, Markaki Y, Olins AL, Olins DE. Phosphatidylserine colocalizes with epichromatin in interphase nuclei and mitotic chromosomes. *Nucleus* (Austin, Tex). 2012;3:200-10. PMID:22555604
- [3] Losman MJ, Fasy TM, Novick KE, Monestier M. Monoclonal autoantibodies to subnucleosomes from a MRL/Mp(−)/+ mouse. Oligoclonality of the antibody response and recognition of a determinant composed of histones H2A, H2B, and DNA. *Journal of immunology* (Baltimore, Md: 1950) 1992;148:1561-9. PMID:1371530
- [4] Mourdjeva M, Kyurkchiev D, Mandinova A, Altankova I, Kehayov I, Kyurkchiev S. Dynamics of membrane translocation of phosphatidylserine during apoptosis detected by a monoclonal antibody. *Apoptosis: an international journal on programmed cell death*. 2005;10:209-17. doi:10.1007/s10495-005-6076-5. PMID:15711937
- [5] Olins AL, Ishaque N, Chotewutmontri S, Langowski J, Olins DE. Retrotransposon Alu is enriched in the epichromatin of HL-60 cells. *Nucleus* (Austin, Tex). 2014;5:237-46. PMID:24824428
- [6] Kalashnikova AA, Porter-Goff ME, Muthurajan UM, Luger K, Hansen JC. The role of the nucleosome acidic patch in modulating higher order chromatin structure. *Journal of the Royal Society, Interface / the Royal Society*. 2013;10:20121022. doi:10.1098/rsif.2012.1022
- [7] Kato H, Jiang J, Zhou BR, Rozendaal M, Feng H, Ghirlando R, Xiao TS, Straight AF, Bai Y. A conserved mechanism for centromeric nucleosome recognition by centromere protein CENP-C. *Science* (New York, NY). 2013;340:1110-3. doi:10.1126/science.1235532
- [8] da Silva IT, de Oliveira PS, Santos GM. Featuring the nucleosome surface as a therapeutic target. *Trends Pharmacol Sci*. 2015;36:263-9. doi:10.1016/j.tips.2015.02.010. PMID:25835595
- [9] Fang Q, Chen P, Wang M, Fang J, Yang N, Li G, Xu RM. Human cytomegalovirus IE1 protein alters the higher-order chromatin structure by targeting the acidic patch of the nucleosome. *eLife*. 2016;5:e11911.
- [10] Armache KJ, Garlick JD, Canzio D, Narlikar GJ, Kingston RE. Structural basis of silencing: Sir3 BAH domain in complex with a nucleosome at 3.0 Å resolution. *Science* (New York, NY). 2011;334:977-82. doi:10.1126/science.1210915
- [11] Kato H, van Ingen H, Zhou BR, Feng H, Bustin M, Kay LE, Bai Y. Architecture of the high mobility group nucleosomal protein 2-nucleosome complex as revealed by methyl-based NMR. *Proc Natl Acad Sci U S A*. 2011;108:12283-8. doi:10.1073/pnas.1105848108. PMID:21730181
- [12] Cuylen S, Blaukopf C, Politi AZ, Muller-Reichert T, Neumann B, Poser I, Ellenberg J, Hyman AA, Gerlich



- DW. Ki-67 acts as a biological surfactant to disperse mitotic chromosomes. *Nature*. 2016;535:308-12. doi:10.1038/nature18610. PMID:27362226
- [13] Fol H. Le quadrille des centres un épisode nouveau dans l'histoire de la fécondation. *Archives des sciences physiques et naturelles* 1891;XXV:393-420..
- [14] Fol H. Die Teilung der Zelle. *Lehrbuch der vergleichenden mikroskopischen Anatomie mit Einschluss der vergleichenden Histologie und Histogenie*. Leipzig: Engelmann. 1896:255-81.
- [15] Olins AL, Herrmann H, Lichter P, Kratzmeier M, Doenecke D, Olins DE. Nuclear envelope and chromatin compositional differences comparing undifferentiated and retinoic acid- and phorbol ester-treated HL-60 cells. *Exp Cell Res*. 2001;268:115-27. doi:10.1006/excr.2001.5269. PMID:11478838
- [16] Mardian JK, Paton AE, Bunick GJ, Olins DE. Nucleosome cores have two specific binding sites for non-histone chromosomal proteins HMG 14 and HMG 17. *Science (New York, NY)* 1980;209:1534-6. doi:10.1126/science.7433974
- [17] Paton AE, Wilkinson-Singley E, Olins DE. Nonhistone nuclear high mobility group proteins 14 and 17 stabilize nucleosome core particles. *The Journal of biological chemistry* 1983;258:13221-9. PMID:6226664
- [18] Mark Welch DBJ, A, Langowski J, Olins AL, Olins DE. Transcriptomes reflect the Phenotypes of Undifferentiated, Granulocyte and Macrophage forms of HL-60/S4 cells. *Nucleus (Austin, Tex)*. 2017;8:222-37. PMID:28152343
- [19] Lieberman-Aiden E, van Berkum NL, Williams L, Imakaev M, Ragoczy T, Telling A, Amit I, Lajoie BR, Sabo PJ, Dorschner MO, et al. Comprehensive mapping of long-range interactions reveals folding principles of the human genome. *Science (New York, NY)*. 2009;326:289-93. doi:10.1126/science.1181369
- [20] Dixon JR, Selvaraj S, Yue F, Kim A, Li Y, Shen Y, Hu M, Liu JS, Ren B. Topological domains in mammalian genomes identified by analysis of chromatin interactions. *Nature*. 2012;485:376-80. doi:10.1038/nature11082. PMID:22495300
- [21] Naumova N, Imakaev M, Fudenberg G, Zhan Y, Lajoie BR, Mirny LA, Dekker J. Organization of the mitotic chromosome. *Science (New York, NY)*. 2013;342:948-53. doi:10.1126/science.1236083
- [22] Baddeley D, Chagin VO, Schermelleh L, Martin S, Pombo A, Carlton PM, Gahl A, Domaing P, Birk U, Leonhardt H, et al. Measurement of replication structures at the nanometer scale using super-resolution light microscopy. *Nucleic Acids Res*. 2010;38:e8. doi:10.1093/nar/gkp901. PMID:19864256
- [23] Markaki Y, Gunkel M, Schermelleh L, Beichmanis S, Neumann J, Heidemann M, Leonhardt H, Eick D, Cremer C, Cremer T. Functional nuclear organization of transcription and DNA replication: a topographical marriage between chromatin domains and the interchromatin compartment. *Cold Spring Harb Symp Quant Biol*. 2010;75:475-92. doi:10.1101/sqb.2010.75.042. PMID:21467142
- [24] Rhind N, Gilbert DM. DNA replication timing. *Cold Spring Harb Perspect Biol*. 2013;5:a010132. doi:10.1101/cshperspect.a010132. PMID:23838440
- [25] Nozaki T, Imai R, Tanbo M, Nagashima R, Tamura S, Tani T, Joti Y, Tomita M, Hibino K, Kanemaki MT, et al. Dynamic Organization of Chromatin Domains Revealed by Super-Resolution Live-Cell Imaging. *Mol Cell*. 2017;67:282-93.e7. doi:10.1016/j.molcel.2017.06.018. PMID:28712725
- [26] Shlomchik M, Mascelli M, Shan H, Radic MZ, Pisetsky D, Marshak-Rothstein A, Weigert M. Anti-DNA antibodies from autoimmune mice arise by clonal expansion and somatic mutation. *J Exp Med*. 1990;171:265-92. doi:10.1084/jem.171.1.265. PMID:2104919
- [27] Radic MZ, Weigert M. Genetic and structural evidence for antigen selection of anti-DNA antibodies. *Annu Rev Immunol*. 1994;12:487-520. doi:10.1146/annurev.iy.12.040194.002415. PMID:8011289
- [28] Krishnan MR, Jou NT, Marion TN. Correlation between the amino acid position of arginine in VH-CDR3 and specificity for native DNA among autoimmune antibodies. *Journal of immunology (Baltimore, Md: 1950)* 1996;157:2430-9. PMID:8805642
- [29] Stanfield RL, Eilat D. Crystal structure determination of anti-DNA Fab A52. *Proteins*. 2014;82:1674-8. doi:10.1002/prot.24514. PMID:24449198
- [30] Kalinina O, Wang Y, Sia K, Radic M, Cazenave PA, Weigert M. Light chain editors of anti-DNA receptors in human B cells. *J Exp Med*. 2014;211:357-64. doi:10.1084/jem.20122340. PMID:24470445
- [31] Neeli I, Richardson MM, Khan SN, Nicolo D, Monestier M, Radic MZ. Divergent members of a single autoreactive B cell clone retain specificity for apoptotic blebs. *Mol Immunol*. 2007;44:1914-21. doi:10.1016/j.molimm.2006.09.027. PMID:17084454
- [32] Li H, Jiang Y, Cao H, Radic M, Prak EL, Weigert M. Regulation of anti-phosphatidylserine antibodies. *Immunity*. 2003;18:185-92. doi:10.1016/S1074-7613(03)00026-8. PMID:12594946
- [33] Radic MZ, Weigert M. Intricacies of anti-DNA autoantibodies. *Journal of immunology (Baltimore, Md: 1950)*. 2004;172:3367; author reply —8. doi:10.4049/jimmunol.172.6.3367. PMID:15004132
- [34] Zhang R, Erler J, Langowski J. Histone Acetylation Regulates Chromatin Accessibility: Role of H4K16 in Internucleosome Interaction. *Biophys J*. 2017;112:450-9. doi:10.1016/j.bpj.2016.11.015. PMID:27931745
- [35] Klein JS, Gnanapragasam PN, Galimidi RP, Foglesong CP, West AP, Jr., Bjorkman PJ. Examination of the contributions of size and avidity to the neutralization mechanisms of the anti-HIV antibodies b12 and 4E10. *Proc Natl Acad Sci U S A*. 2009;106:7385-90. doi:10.1073/pnas.0811427106. PMID:19372381
- [36] De Michele C, De Los Rios P, Foffi G, Piazza F. Simulation and Theory of Antibody Binding to Crowded



- Antigen-Covered Surfaces. *PLoS Comput Biol*. 2016;12:e1004752. doi:10.1371/journal.pcbi.1004752. PMID:26967624
- [37] Jamin A, Wiebe MS. Barrier to Autointegration Factor (BANF1): interwoven roles in nuclear structure, genome integrity, innate immunity, stress responses and progeria. *Curr Opin Cell Biol*. 2015;34:61-8. doi:10.1016/j.ceb.2015.05.006. PMID:26072104
- [38] Schooley A, Vollmer B, Antonin W. Building a nuclear envelope at the end of mitosis: coordinating membrane reorganization, nuclear pore complex assembly, and chromatin de-condensation. *Chromosoma*. 2012;121:539-54. doi:10.1007/s00412-012-0388-3. PMID:23104094
- [39] Wandke C, Kutay U. Enclosing chromatin: reassembly of the nucleus after open mitosis. *Cell*. 2013;152:1222-5. doi:10.1016/j.cell.2013.02.046. PMID:23498932
- [40] Teif VB, Mallm JP, Sharma T, Mark Welch DB, Rippe K, Eils R, Langowski J, Olins AL, Olins DE. Nucleosome repositioning during differentiation of a human myeloid leukemia cell line. *Nucleus (Austin, Tex)*. 2017;8:188-204. PMID:28406749
- [41] Hammermann M, Toth K, Rodemer C, Waldeck W, May RP, Langowski J. Salt-dependent compaction of di- and trinucleosomes studied by small-angle neutron scattering. *Biophys J*. 2000;79:584-94. doi:10.1016/S0006-3495(00)76318-1. PMID:10866982
- [42] Hell SW, Wichmann J. Breaking the diffraction resolution limit by stimulated emission: stimulated-emission-depletion fluorescence microscopy. *Opt Lett*. 1994;19:780-2. doi:10.1364/OL.19.000780. PMID:19844443
- [43] Gould TJ, Burke D, Bewersdorf J, Booth MJ. Adaptive Optics Enables 3D STED Microscopy in Aberrating Specimens. *Optics Express*. 2012;20:20998-1009. doi:10.1364/OE.20.020998. PMID:23037223
- [44] Gould TJ, Kromann EB, Burke D, Booth MJ, Bewersdorf J. Auto-aligning stimulated emission depletion microscope using adaptive optics. *Opt Lett*. 2013;38:1860-2. doi:10.1364/OL.38.001860. PMID:23722769
- [45] Vicidomini G, Moneron G, Han KY, Westphal V, Ta H, Reuss M, Engelhardt J, Eggeling C, Hell SW. Sharper low-power STED nanoscopy by time gating. *Nat Methods*. 2011. doi:10.1038/nmeth.1624. PMID:21642963